INTERNATIONAL JOURNAL FOR NUMERICAL METHODS IN FLUIDS, VOL. 25, 265–283 (1997)

AUGMENTED LAGRANGIAN METHOD AND OPEN BOUNDARY CONDITIONS IN 2D SIMULATION OF POISEUILLE–BÉNARD CHANNEL FLOW

X. NICOLAS,[1] P. TRAORE,[1] A. MOJTABI[1]* AND J. P. CALTAGIRONE[2]

[1]*Institut de Mécanique des Fluides de Toulouse, UMR CNRS/INP-UPS 5502, Avenue Professeur Camille Soula, F-31400 Toulouse, France*
[2]*Laboratoire MASTER, ENSCPB, Avenue Pey-Berland, BP 108 F-33402 Talence Cedex, France*

SUMMARY

The main objective of this study is to compare the influence of different boundary conditions upon the incompressible Poiseuille–Bénard channel flow (PBCF) in a 2D rectangular duct heated from below. In a first technical part the algorithm used to carry out this work, based on the augmented Lagrangian method, is presented. The implementation details of the five different open boundary conditions (OBCs) and the periodic boundary conditions (PBCs) tested in the present paper are also given. The study is then carried out for $1800 < Ra \leqslant 10{,}000$, $0 < Re \leqslant 10$ and $0{\cdot}67 \leqslant Pr \leqslant 6{\cdot}4$. The five selected OBCs, applied at the outlet of the computational domain, respectively express the following conditions: a square profile for the velocity (OBC1), mass conservation (OBC2), zero second derivative of the horizontal velocity component (OBC3), a mixed boundary condition combining Dirichlet and Neumann conditions (OBC4) and an Orlanski-type boundary condition (OBC5). A good estimation of the perturbation amplitude and of the length of the perturbed zone at the outlet boundary is proposed. It is shown that OBC5 causes very little perturbation in the recirculating flow compared with the other OBCs. © 1997 by John Wiley & Sons, Ltd.

Int. J. Numer. Meth. Fluids, **25**: 265–283 (1997).

No. of Figures: 8. No. of Tables: 2. No. of References: 30.

KEY WORDS: open boundary conditions; Poiseuille–Bénard flow; augmented Lagrangian; thermal instabilities

INTRODUCTION

Often in computational fluid dynamics (CFD), to compute an outflow, one encounters the problem of open boundary conditions (OBCs). Computational time costs and memory limitations do not permit simulations on large physical domains. To solve the problem mathematically, the domain must be truncated and confined between artificial boundaries onto which numerical conditions are introduced, depending on the nature of the governing equations. However, it is difficult to establish these boundary conditions when the studied fluid system is isolated from the effects of its environment; information about the dynamics of the fluid through the boundary is all the more necessary as the flow is of an elliptic nature (i.e. is made of eddies and recirculations). The OBCs are the result of

* Correspondence to: A. Mojtabi, Institut de Mécanique des Fluides de Toulouse, UMR CNRS/INP-UPS 5502, Avenue Professeur Camille Soula, F-31400 Toulouse, France

CCC 0271–2091/97/030265–19 $17.50

Received 6 June 1995
Revised 23 September 1996

assumptions which do not reflect exactly the real physical phenomenon; if they are not properly chosen, they can have spurious effects such as numerical instabilities, reflections at the boundary and, generally, errors that can propagate and alter the results throughout all the computational domain. Thus the choice of good OBCs is crucial in CFD. This choice is closely linked to the physical behaviour of the flow and to the method used to solve the problem.

The main objective of this paper is to study the influence of five different OBCs, at the outlet of the computational domain, upon the thermoconvective structures that are liable to develop when simulating incompressible Poiseuille–Bénard channel flow (PBCF). The PBCF is a mixed convection flow in a horizontal rectangular channel heated from below. If there is no heating and the channel is open, it is a simple Poiseuille flow. If vertical walls close each end of the channel and if the vertical temperature gradient is sufficiently high ($Ra > 1708$, where Ra is the Rayleigh number), it is a thermoconvective Bénard flow. For three-dimensional channels, when the two phenomena are added, the flow structure is quite complex. For a given Prandtl number Pr and a given aspect ratio of the duct, several types of thermoconvective structures, depending on Ra and Re (where Re is the Reynolds number), can be observed: there can be either transversal rolls, longitudinal rolls (i.e. thermoconvective rolls with their axes either orthogonal or parallel to the axis of the channel) or intermittent patterns.

The stability of these different configurations is a very interesting problem; this has given rise to many theoretical[1–7] and experimental[1,4,8–11] papers. To our knowledge, only two similar papers[12,13] have recently presented results obtained by means of direct three-dimensional numerical simulation. Other works,[14–16] carried out in the frame of CVD (chemical vapour deposition), have mainly focused on heat transfer enhancement related to different thermoconvective structures. When studying their stability numerically, several difficulties appear: it is necessary to ensure, first, that the amplitude of the perturbation caused by the OBC does not cause bifurcations between the different types of thermoconvective structures (transversal or longitudinal rolls) and, second, that the length of the perturbed zone above the outlet is limited compared with the length of the computational domain.

In the present paper the analysis of the influence of OBCs is limited to the two-dimensional PBCF. In this case the flow structure consists of two-dimensional contra-rotative rolls with their axes transversal to the direction of the average channel flow and moving away with the mean flow. The purpose of this study is to determine the OBC which causes the smallest perturbation among the five selected ones. With this aim in view, the five OBCs are all compared with a benchmark solution of the PBCF that was computed by Evans and Paolucci[17] for $Re = 10$, $Ra = 10{,}000$ and $Pr = \frac{2}{3}$. They are also compared with simulations involving periodic boundary conditions (PBCs). The Nusselt number, the variation of the transversal roll wavelength λ and the time period τ are presented for the different OBCs. Several criteria are also proposed for estimating the length of the perturbed zone and the amplitude of the perturbation; their evolution as a function of the Rayleigh and Reynolds numbers is studied for the following range of dimensionless parameters: $0 < Re \leqslant 10$, $1800 < Ra \leqslant 10{,}000$ and $0{\cdot}67 \leqslant Pr \leqslant 6{\cdot}4$.

The 2D PBCF was already proposed by Sani and Gresho[18] as a test case for an OBC minisymposium that took place in Swansea, U.K. on 10 July 1989. Bottaro[19] and Kobayashi *et al.*[20] compared different OBCs with Evans and Paolucci's benchmark solution. Other test cases were proposed during the minisymposium; the summary and remarks of this event are described in Reference 18.

As mentioned before, the choice of the OBCs is partly linked to the method used to compute the solution of the problem. For the present work a finite volume numerical code based on the augmented Lagrangian method has been developed. This method consists of an optimization technique to determine a velocity–pressure saddle point under the incompressibility constraint $\nabla \cdot \mathbf{V} = 0$; the saddle point is computed by an iterative algorithm of Uzawa type.[21,22] This method at present is not

frequently used. However, our experience in CFD has shown that it is very efficient in comparison with the classical numerical schemes: it permits us to simulate flows with important constraints or with strong variations in the control parameters and in the geometry, for which other methods diverge. The augmented Lagrangian method was formulated in the publications by Fortin and Glowinski[23] and Glowinski,[24] in which a variety of problems in the fields of fluid mechanics and elasticity are treated. The first part of this paper presents the main outlines of the method. For more details see References 23–26, in which numerous remarks on the implementation of the algorithm are available.

NUMERICAL PROCEDURE

Governing equations

The problem is formulated considering the usual hypotheses for a Newtonian and incompressible fluid and the Boussinesq approximation is assumed to be valid. The three conservation equations (continuity, momentum and energy equations), provided with adequate initial and boundary conditions, enable us to express the solution of the PBCF. In primitive variables (velocity $\mathbf{V}$, pressure P, temperature T) and under its dimensionless form the system that has to be solved takes the following expression:

$$\text{(I)}\begin{cases} \nabla \cdot \mathbf{V} = 0, & (1)\\ \dfrac{\partial \mathbf{V}}{\partial t} + (\mathbf{V}\cdot\nabla)\mathbf{V} = -\nabla P + \dfrac{1}{Re}\Delta\mathbf{V} + \dfrac{Ra}{Re^2 Pr}T\mathbf{k}, & (2)\\ \dfrac{\partial T}{\partial t}\mathbf{V}\cdot\nabla T + \dfrac{1}{RePr}\Delta T. & (3) \end{cases}$$

The reference length, velocity, temperature and pressure for scaling are the height H of the duct, the average velocity V^{o} of the PBCF, the temperature difference $T_{\mathrm{hot}} - T_{\mathrm{cold}}$ between the bottom and the top of the channel and $\rho^{\mathrm{o}}V^{\mathrm{o}}$ (where ρ^{o} is the mass per unit volume of the fluid) respectively. Thus $Re = V^{\mathrm{o}}H/v$ is the Reynolds number, $Ra = g\beta(T_{\mathrm{hot}} - T_{\mathrm{cold}})H^3/v\alpha$ is the Rayleigh number and $Pr = v/\alpha$ is the Prandtl number. Here v, β and α are the kinematic viscosity, thermal expansion coefficient and thermal diffusion coefficient of the fluid respectively. g is the gravity constant and $\mathbf{k}$ is the vertical unit vector.

The time scheme used to solve (I) is Gear's second-order backward implicit scheme ($(a, b, c) = (1{\cdot}5, 2, -0{\cdot}5)$ in system (II) below). The time discretization being uniform, the time step is denoted Δt; the current time and the following time step (time at which the fields are unknown) are $n\Delta t$ and $(n+1)\Delta t$ respectively. The superscripts of the primitive variables correspond to the time index. In the momentum equation the buoyancy term $RaT\mathbf{k}/Re^2Pr$ is treated explicitly; therefore the two coupled equations (2) and (3) are solved separately. The advective term $(\mathbf{V}\cdot\nabla)\mathbf{V}$ being linearized, the time-discretized form of (I) consists of computing $(\mathbf{V}^{n+1}, P^{n+1}, T^{n+1})$ as follows:

$$\text{(II)}\begin{cases} \nabla \cdot \mathbf{V}^{n+1} = 0, & (4)\\ A^n\mathbf{V}^{n+1} + \nabla P^{n+1} = \mathbf{F}, & (5)\\ BT^{n+1} = G, & (6) \end{cases}$$

where

$$A^n = \frac{a}{\Delta t} + \mathbf{V}^n \cdot \nabla - \frac{1}{Re}\Delta,$$

$$\mathbf{F} = \frac{Ra}{Re^2 Pr} T^n \mathbf{k} + \frac{b\mathbf{V}^n + c\mathbf{V}^{n-1}}{\Delta t},$$

$$B = \frac{a}{\Delta t} + \mathbf{V}^{n+1} \cdot \nabla - \frac{1}{RePr}\Delta,$$

$$G = \frac{bT^n + cT^{n-1}}{\Delta t}.$$

Augmented Lagrangian algorithm

In system (II) the main difficulties occur in the computation of equations (4) and (5); these difficulties are due to the velocity–pressure coupling, the treatment of the continuity constraint $\nabla \cdot \mathbf{V} = 0$ and the determination of boundary conditions on pressure. It could be argued that the coupled linear system in $(\mathbf{V}, P)$ corresponding to equations (4) and (5) can be solved directly; however, the associated matrix is often very large and very ill-conditioned, making it difficult to ensure the stability and convergence of the iterative solver for the linear system. It is often preferred to separate the computation of the velocity from that of the pressure. Here this is achieved by using the augmented Lagrangian method.[23,24]

It has been shown[23,24] that the variational formulation of the problem 'to find $(\mathbf{V}, P)$ in order that (4) and (5) are satisfied' consists of minimizing a functional (derived from the momentum equation) under the incompressibility constraint $\nabla \cdot \mathbf{V} = 0$. This minimization problem is equivalent to solving a saddle point search problem for $(\mathbf{V}, P)$ after having introduced the augmented Lagrangian associated with the functional and the constraint defined above. The determination of the saddle point $(\mathbf{V}, P)$ is obtained by the iterative Uzawa algorithm.[21,22] $(\mathbf{V}^n, P^n)$ being known, $(\mathbf{V}^{n+1}, P^{n+1})$ are obtained using the following external loop with iteration index k (time index is n):

$$\text{(III)} \begin{cases} (\mathbf{V}^{k=0}, P^{k=0}) = (\mathbf{V}^n, P^n), \\ A_r^k \mathbf{V}^{k+1} = \mathbf{F}^n - \nabla P^k, & (7) \\ P^{k+1} = P^k - s(\nabla \cdot \mathbf{V}^{k+1}), & (8) \\ \text{when} \quad \|\nabla \cdot \mathbf{V}^{k+1}\| < \varepsilon, \quad \text{then} \quad (\mathbf{V}^{n+1}, P^{n+1}) = (\mathbf{V}^{k+1}, P^{k+1}). \end{cases}$$

In equation (7), $A_r^k = A^k - r\nabla(\nabla \cdot)$. The additional operator $-r\nabla(\nabla \cdot)$ comes from the augmented Lagrangian and takes into account the incompressibility constraint; its function is to increase the rate of convergence of algorithm (III). Here r, s and ε are three positive constants; ε has a small value and is used to determine the convergence criterion (in this paper all the results were obtained with $\varepsilon = 10^{-5}$). $\|\nabla \cdot \mathbf{V}^{k+1}\|$ represents the arithmetic mean of the absolute values of $\nabla \cdot \mathbf{V}$ at each mesh point.

Fortin and Glowinski[23] show that the convergence condition for algorithm (III) is $0 < s < 2(r + 1/Re)$. They also prove that a greater rate of convergence of (III) is achieved as r increases; on the other hand, the bigger r is, the more ill-conditioned the matrix of the linear system (derived from A_r^k in equation (7)) will be. Thus the choice of r must be a compromise in relation to two conflicting requirements: minimizing the number of iterations on k and minimizing the number of iterations necessary to solve the linear system. Note that when very small time steps are used (e.g. for unsteady problems), the matrix of the system becomes more diagonally dominant and it is

possible to increase the value of r. Fortin and Glowinski experimentally show,[23] by several numerical tests, that the optimum rate of convergence is approximately obtained when s is slightly bigger than r, when r is large. Thus, in this research, after having tested several values of r and s between 10 and 5000, we chose $r = 400$ and $s = 500$ when $\Delta t = 0{\cdot}0005$. The complete algorithm, to move from time $n\Delta t$ to time $(n+1)\Delta t$, is presented in Figure 1.

The augmented Lagrangian term $-r\nabla(\nabla \cdot \mathbf{V}^{k+1})$ couples the velocity components and subsequently adds eight diagonals (in 2D problems) in the matrix associated with A_r^k. Therefore a highly efficient method has to be used to solve the linear system derived from (7), since U and W must be calculated at the same time. Since the discretization of the advective term $(\mathbf{V} \cdot \nabla)\mathbf{V}$ makes the linear system matrix non-symmetric and since it is a regular matrix, the Bi-CGSTAB (bi-conjugate stabilized gradient) method[27] with a preconditioning based on a modified and incomplete Gauss factorization MILU[28] was the chosen solver. The same solver is used to compute T from the linear system derived from (6).

The space discretization of the momentum equation (7) and energy equation (6) is generated by using a finite control volume method on a staggered grid.[29] This grid is Cartesian and uniform in each space direction, with the space step Δx in the horizontal direction and Δz in the vertical direction. P and T are computed at the nodes of the control volumes; U and W, the horizontal and vertical velocity components, are computed at the centre of the horizontal (resp. vertical) edges of the control volumes (see Figure 2). A central difference scheme is used for the space discretization of the convective fluxes, while the diffusive fluxes are discretized with central second-order derivative approximations.

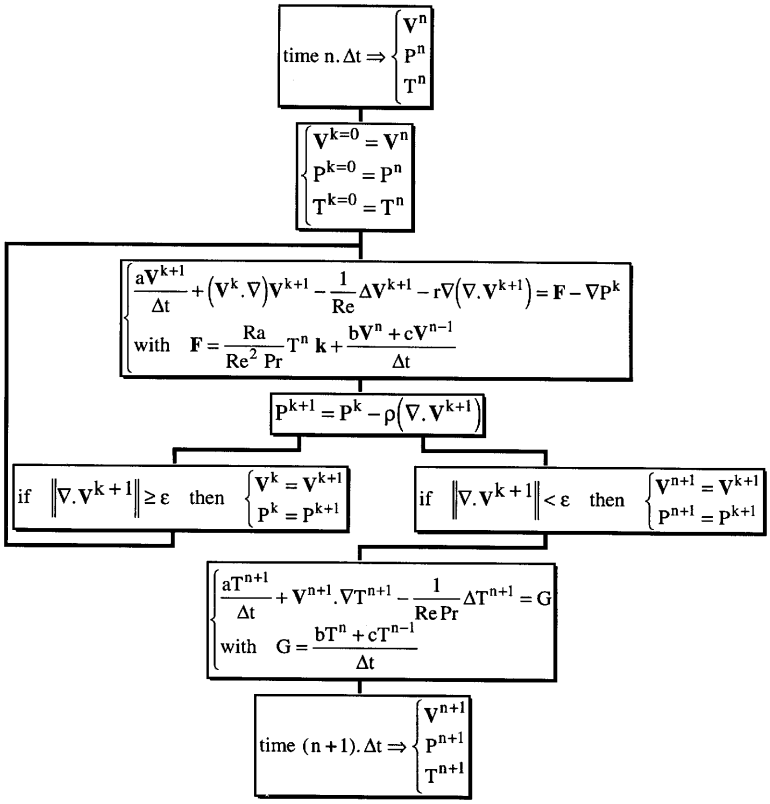

Figure 1. Augmented Lagrangian algorithm

We note that the finite volume method leads to the following discretized equation for each control volume:[29]

$$a_P(\phi)\phi_P = a_E(\phi)\phi_E + a_N(\phi)\phi_N + a_W(\phi)\phi_W + a_S(\phi)\phi_S + b(\phi), \tag{9}$$

where ϕ stands for one of the three variables T, U or W and $a_i(\phi)$ (with $i = P, E, N, W, S$) and $b(\phi)$ are coefficients depending on the discretization scheme. The subscript P refers to the central control volume point (i, k) and subscripts E, N, W and S refer to its neighbouring points to the east, north, west and south respectively (see Figure 2).

To be able to compute the linear system corresponding to (9) for all the control volumes, equation (9) must be verified everywhere, even at the outlet boundary. However, this is not always possible when, for example, ϕ_E is unknown on this boundary. To solve the problem, OBCs are implemented. In this paper, two formulations have been used. The 'weak formulation' consists of expressing ϕ_E from the discretized form of the OBC and introducing it in equation (9). For instance, in the case of

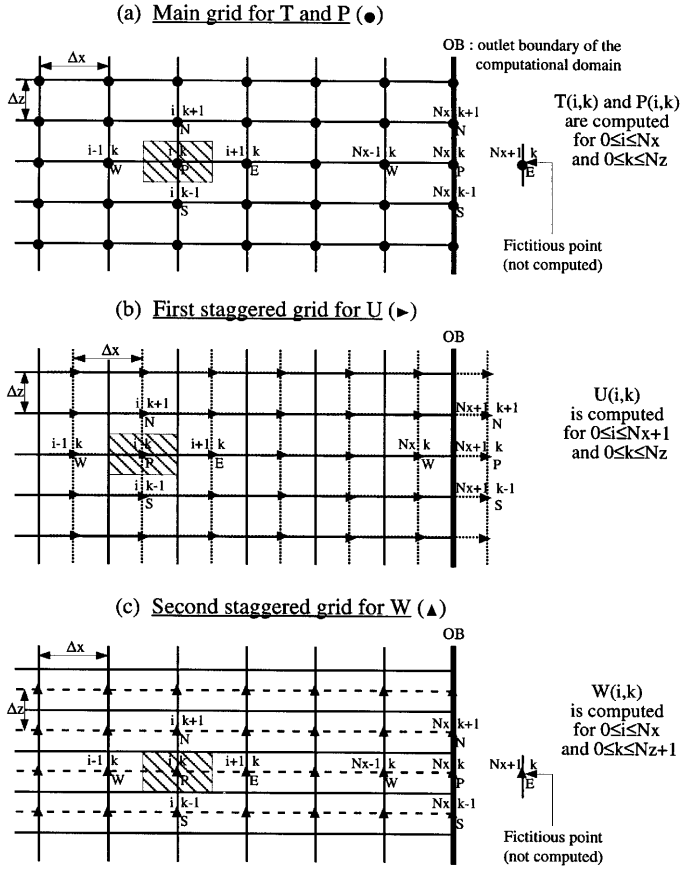

Figure 2. Grid system and positioning of variables ((a) T and P; (b) U; (c) W) near outlet of computational domain

Figure 2(a) or 2(c), applying the Neumann boundary condition $\partial\phi/\partial x = 0$ gives $\phi_E = \phi_W$. By introducing this expression in (9), the coefficients are modified in the following way:

$$a_W(\phi) = a_W(\phi) + a_E(\phi),$$
$$a_E(\phi) = 0,$$
$$a_P(\phi), a_N(\phi), a_S(\phi) \quad \text{and} \quad b(\phi) \text{ remain unchanged.}$$

The 'strong formulation' consists of directly identifying the discretized form of the OBC with equation (9). For instance, in the case of Figure 2(b) the Neumann condition gives $\phi_P = \phi_E$. Then the coefficients are

$$a_P(\phi) = a_E(\phi) = 1,$$
$$a_N(\phi) = a_W(\phi) = a_S(\phi) = b(\phi) = 0.$$

So far, no hypothesis has been made about the nature and geometry of the flow; it has only been assumed that the system was provided with adequate initial and boundary conditions in order to be solved. The conditions that have been implemented to compute the PBCF are presented in the following subsection. Note that one of the advantages of Uzawa's algorithm (III) (compared e.g. with the classical SIMPLE, SIMPLER, PISO, etc. methods) is that no boundary condition on pressure is required. Indeed, owing to the explicit treatment of P in (8), only the initial conditions for pressure (and the entire velocity field) are needed to compute P at each time step.

Computational configurations and boundary conditions

Two main computational configurations have been used to compute the PBCF. The first one is a rectangular channel with one of the five tested OBCs at the outlet and a conductive Poiseuille flow at the inlet; the second one is a rectangular channel with PBCs. The description of these configurations and the method used to implement the different OBCs or the PBCs are given below.

First configuration. This is illustrated in Figure 3 and its initial and boundary conditions for ($\mathbf{V}$, P, T) are given in Table I (except for the five OBCs, whose definition and implementation are given in the next subsection).

This configuration allows us to observe the space amplification of the perturbation until non-linear saturation occurs.[5] When thermoconvection develops in the PBF, three zones can be distinguished (see Figure 3): (i) for $0 \leqslant x \leqslant x_{in}$, the inlet zone in which the perturbation is growing; then, after its saturation, (ii) for $x_{in} \leqslant x \leqslant x_{out}$, a fully established periodic flow of transversal rolls; and (iii) near

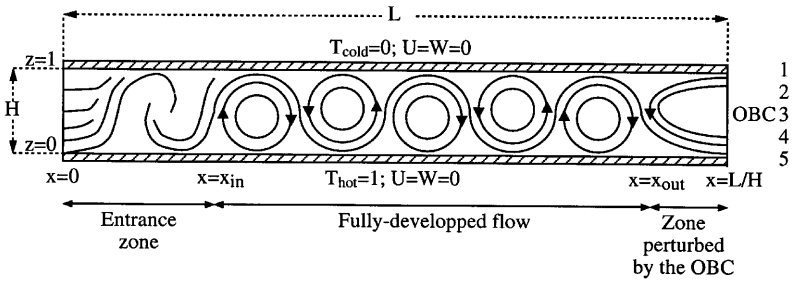

Figure 3. First computational configuration with conductive Poiseuille flow at inlet and one of five tested OBCs at outlet

Table I. Inlet, bottom and top boundary conditions as well as initial conditions for first computational configuration (with OBC)

Inlet BC ($x=0$)	Bottom BC ($z=0$)	Top BC ($z=1$)	Initial condition ($t=0$)
$U(0, z, t)=-6(z^2-z)$	$U(x, 0, t)=0$	$U(x, 1, t)=0$	$U(x, z, 0)=-6(z^2-z)$
$W(0, z, t)=0$	$W(x, 0, t)=0$	$W(x, 1, t)=0$	$W(x, z, 0)=0$
$T(0, z, t)=1-z$	$T(x, 0, t)=1$	$T(x, 1, t)=0$	$T(x, z, 0)=0$
No BC for P	No BC for P	No BC for P	$P(x, z, 0)=1-x$

the outlet, for $x_{\text{out}} \leqslant x \leqslant L/H$, the zone on which we are going to focus, where the rolls are more or less distorted by the OBC (the longer this zone is, the more spurious the effect of the OBC).

Note that the length of the inlet and of the outlet can vary according to the values of Ra, Re and Pr. Therefore computational domains with different aspect ratios L/H (where L and H are the length and height of the duct respectively) are used to obtain a fully developed periodic flow for each computed case. For the test case proposed by Evans and Paolucci[17] ($Ra=10{,}000$, $Re=10$, $Pr=\frac{2}{3}$), $x_{\text{in}} \approx 2$; therefore we chose $L/H=5$ and for the space and time steps we took $(\Delta x, \Delta z, \Delta t)=(0{\cdot}0725, 0{\cdot}05, 0{\cdot}0005)$. For $Pr=6{\cdot}4$, when $(Ra, Re)=(4700, 0{\cdot}18)$ and $(4700, 3)$, we chose $L/H=10$; but, when $(Ra, Re)=(1804, 0{\cdot}18)$, we took $L/H=20$, because $x_{\text{in}} \approx 9$. In all cases with $Pr=6{\cdot}4$, $(\Delta x, \Delta z, \Delta t)=(0{\cdot}1, 0{\cdot}05, 0{\cdot}0005)$ unless stated otherwise.

OBCs at outlet of first configuration. Many OBCs are used by the CFD research community. Frequently their physical interpretation is difficult, but they permit one to close a problem mathematically. When simulating a flow, no clear criterion permits one to select one of these OBCs over the others; the only way to proceed is to analyse the behaviour of the flow *a posteriori*. Subsequently we decided to test five of the most commonly encountered OBCs. Their definitions and the ways in which they are implemented are given below. Note that the strong formulation is used to implement the OBCs for U, while the weak formulation is used for W (except for OBC1) and T.

OBC1

$$U = V^{\text{o}}, \qquad W = 0, \qquad \frac{\partial T}{\partial x} = 0,$$

where

$$V^{\text{o}} = \int_{z=0}^{z=1} -6(z^2 - z)\mathrm{d}z$$

is the average velocity of the flow. To be more precise, in order to take into account both the no-slip condition on the horizontal plates of the channel and the mass conservation, we took $U(i, 0)=U(i, Nz)=0$ and $U(i, k)=[Nz/(Nz-1)]V^{\text{o}}$ for $0<k<Nz$ (Nz is the total number of meshes in the z-direction).

OBC1 is a coarse way to simulate the porous side walls[8,12] that are often placed at the inlet and outlet of experimental channels in order to avoid direct contact of the measurement zone with the feed pump.

OBC2

$$\frac{\partial U}{\partial x} = -\frac{\partial W}{\partial z}, \qquad \frac{\partial W}{\partial x} = 0, \qquad \frac{\partial T}{\partial x} = 0.$$

The discretization of the condition for U gives (see Figure 2(b))

$$U^{k+1}(Nx+1,k) - U^{k+1}(Nx,k) = -(\Delta x/\Delta z)[W^n(Nx,k+1) - W^n(Nx,k)].$$

In the strong formulation this expression implies

$$\begin{aligned} a_{\mathrm{P}}(U) &= a_{\mathrm{W}}(U) = 1, \\ b(U) &= -(\Delta x/\Delta z)[W^n(Nx,k+1) - W^n(Nx,k)], \\ a_{\mathrm{E}}(U) &= a_{\mathrm{N}}(U) = a_{\mathrm{S}}(U) = 0. \end{aligned}$$

OBC2 is directly obtained by applying the conservation of mass at the outlet boundary. We have verified (not shown here) that OBC2 has exactly the same influence on the numerical solution (same profiles of U, W and T at the outlet, same amplitude of perturbations, same perturbed length, etc.) as a Neumann boundary condition on U, W and T. The only difference is that the computational time is shorter with OBC2. Indeed, with the augmented Lagrangian algorithm, a larger number of loops in k (see system (III) or Figure 1) is necessary to reach the convergence criterion $\|\nabla \cdot \mathbf{V}\| < \varepsilon$ when using the simple Neumann condition. This criterion is more easily verified by OBC2 since it ensures the continuity equation on the boundary. OBC2 must be seen here as a means to close the problem mathematically.

OBC3

$$\frac{\partial^2 U}{\partial x^2} = 0, \qquad \frac{\partial W}{\partial x} = 0, \qquad \frac{\partial T}{\partial x} = 0.$$

$U^{k+1}(Nx+1,k)$ is obtained explicitly by discretizing the condition for U with a second-order upwind scheme in space:

$$U^{k+1}(Nx+1,k) = 2{\cdot}5U^n(Nx,k) - 2U^n(Nx-1,k) + 0{\cdot}5U^n(Nx-2,k).$$

Therefore

$$\begin{aligned} a_{\mathrm{P}}(U) &= 1, \\ b(U) &= 2{\cdot}5U^n(Nx,k) - 2U^n(Nx-1,k) + 0{\cdot}5U^n(Nx-2,k), \\ a_{\mathrm{E}}(U) &= a_{\mathrm{W}}(U) = a_{\mathrm{N}}(U) = a_{\mathrm{S}}(U) = 0. \end{aligned}$$

Note that the semi-implicit treatment of this OBC implies an ill-conditioning of the linear system matrix: $a_{\mathrm{P}}(U) = 1$ and $a_{\mathrm{W}}(U) = 2{\cdot}5$.

OBC3 is less restrictive than the Neumann boundary condition: whereas the latter implies a constant extrapolation of U at the outlet boundary, OBC3 can be seen as a linear extrapolation of U on this boundary. Note that a second-order derivative was also tested for T, but the results were never as good as those obtained with the first-order derivative.

OBC4

$$\frac{\partial U}{\partial x} = -\beta_U(U - U_\infty), \qquad \frac{\partial W}{\partial x} = -\beta_W(W - W_\infty), \qquad \frac{\partial T}{\partial x} = -\beta_T(T - T_\infty).$$

For U the discretization gives (see Figure 2(b))

$$U^{k+1}(Nx+1,k) - U^{k+1}(Nx,k) = -\Delta x \beta_U \{[U^{k+1}(Nx+1,k) + U^{k+1}(Nx,k)]/2 - U_\infty(k)\}$$

and the strong formulation implies

$$\begin{aligned} a_{\mathrm{P}}(U) &= 1 + \Delta x \beta_U/2, \\ a_{\mathrm{W}}(U) &= 1 - \Delta x \beta_U/2, \\ b(U) &= \Delta x \beta_U U_\infty(k), \\ a_{\mathrm{E}}(U) &= a_{\mathrm{N}}(U) = a_{\mathrm{S}}(U) = 0. \end{aligned}$$

For W the discretization gives (see Figure 2(c))

$$W^{k+1}(Nx+1,k) - W^{k+1}(Nx-1,k) = -2\Delta x \beta_W [W^{k+1}(Nx,k) - W_\infty(k)]$$

and the weak formulation implies

$$\begin{aligned} a_{\mathrm{W}}(W) &= a_{\mathrm{W}}(W) + a_{\mathrm{E}}(W), \\ a_{\mathrm{P}}(W) &= a_{\mathrm{P}}(W) + 2\Delta x \beta_W a_{\mathrm{E}}(W), \\ b(W) &= b(W) + 2\Delta x \beta_W W_\infty(k) a_{\mathrm{E}}(W), \\ a_{\mathrm{E}}(W) &= 0, \\ a_{\mathrm{N}}(W) \quad &\text{and} \quad a_{\mathrm{S}}(W) \text{ remain unchanged.} \end{aligned}$$

OBC4 is a Fourier-type boundary condition: this is a mixed condition between Neumann and Dirichlet conditions. In the case of open flows (e.g. flows around an obstacle) it permits the connection of the recirculating local flow with the fully established parallel flow at infinity, $(U_\infty, W_\infty, T_\infty)$, by adjusting the three positive constants $(\beta_U, \beta_W, \beta_T)$. In the case of channel flows, $(U_\infty, W_\infty, T_\infty)$ generally represent the upstream non-perturbed flow. In the present paper they represent the thermally stratified Poiseuille flow: $U_\infty = -6(z^2 - z)$, $W_\infty = 0$ and $T_\infty = 1 - z$.

Neumann boundary conditions are obtained when $(\beta_U, \beta_W, \beta_T) = (0, 0, 0)$ and Dirichlet boundary conditions when $(\beta_U, \beta_W, \beta_T) = (\infty, \infty, \infty)$. By choosing $(\beta_U, \beta_W, \beta_T)$ between these two limits, the outlet behaviour of the flow can be considerably improved. Since the three constants depend on the nature of the flow and on the chosen non-dimensionalization, the best compromise for $(\beta_U, \beta_W, \beta_T)$ cannot be obtained by a straightforward theoretical principle; it can only be obtained by numerical experiments. For the present work, after having tested and compared several sets of $(\beta_U, \beta_W, \beta_T)$, the optimal value of the triplet was found to be $(\beta_U, \beta_W, \beta_T) \approx (5, 5, 0)$.

OBC5

$$\frac{\partial U}{\partial t} + V^{\mathrm{o}} \frac{\partial U}{\partial x} = 0, \qquad \frac{\partial W}{\partial t} + V^{\mathrm{o}} \frac{\partial W}{\partial x} = 0, \qquad \frac{\partial T}{\partial t} + V^{\mathrm{o}} \frac{\partial T}{\partial x} = 0.$$

For U the discretization gives

$$\frac{U^{k+1}(Nx+1,k) + U^{k+1}(Nx,k) - U^n(Nx+1,k) - U^n(Nx,k)}{2\Delta t} + \frac{V^{\mathrm{o}}}{\Delta x}[U^{k+1}(Nx+1,k) - U^{k+1}(Nx,k)] = 0,$$

which implies

$$\begin{aligned} a_{\mathrm{P}}(U) &= V^{\mathrm{o}} + \Delta x/2\Delta t, \\ a_{\mathrm{W}}(U) &= V^{\mathrm{o}} - \Delta x/2\Delta t, \\ b(U) &= [U^n(Nx+1,k) + U^n(Nx,k)]\Delta x/2\Delta t, \\ a_{\mathrm{E}}(U) &= a_{\mathrm{N}}(U) = a_{\mathrm{S}}(U) = 0. \end{aligned}$$

For W the discretization gives

$$\frac{W^{k+1}(Nx,k) - W^n(Nx,k)}{\Delta t} + \frac{V^{\mathrm{o}}}{2\Delta x}[W^{k+1}(Nx+1,k) - W^{k+1}(Nx-1,k)] = 0,$$

which implies

$$\begin{aligned} a_{\mathrm{W}}(W) &= a_{\mathrm{W}}(W) + a_{\mathrm{E}}(W), \\ a_{\mathrm{P}}(W) &= a_{\mathrm{P}}(W) + (2\Delta x/V^{\mathrm{o}}\Delta t)a_{\mathrm{E}}(W), \\ b(W) &= b(W) + (2\Delta x/V^{\mathrm{o}}\Delta t)W^n(Nx,k)a_{\mathrm{E}}(W), \\ a_{\mathrm{E}}(W) &= 0, \\ a_{\mathrm{N}}(W) \quad &\text{and} \quad a_{\mathrm{S}}(W) \quad \text{remain unchanged.} \end{aligned}$$

This boundary condition is a derived and simplified form of Orlanski's boundary condition.[30] It was initially introduced by Bottaro[19] and later tested by Kobayashi *et al.*[20] on the same configuration as the one used by us. OBC5 can be seen as an approximation of the momentum equation on the boundary; U, W and T are convected by a transport equation whose celerity is the average velocity V^{o} of the flow (V^{o} being defined above). In this way the reflection of these quantities when passing through the boundary is expected to be avoided.

Second configuration with PBCs (periodic boundary conditions). To try to free ourselves from the problem of OBCs, we have computed the PBCF with PBCs since this flow is spatially and temporally periodic when it is fully developed. When implementing PBCs, it is no longer possible to induce the flow in the channel by enforcing a Poiseuille flow at the inlet; now it is induced by imposing a constant pressure gradient ΔP^{o} between the inlet and outlet boundaries during all the computation. Taking ΔP^{o} as the new scaling factor for pressure (instead of $\rho^{\mathrm{o}}V^{\mathrm{o}}$), the boundary conditions for pressure are $P = 1$ at the inlet and $P = 0$ at the outlet. Taking $(\Delta P^{\mathrm{o}}/\rho^{\mathrm{o}})^{1/2}$ as the new scaling factor for velocity (instead of V^{o}), the Reynolds number in system (I) is now defined by $Re = (\Delta P^{\mathrm{o}}/\rho^{\mathrm{o}})^{1/2}H/v$.

The periodicity for $\mathbf{V}$ and T is assumed in the following way: at each time step $(n+1)\Delta t$, $(\mathbf{V}^n, T^n)$ obtained at time step $n\Delta t$ in the centre of the duct ($x = L/2H$) is simultaneously enforced as a boundary condition at the inlet and outlet of the channel (see Figure 4); in this way, at any moment,

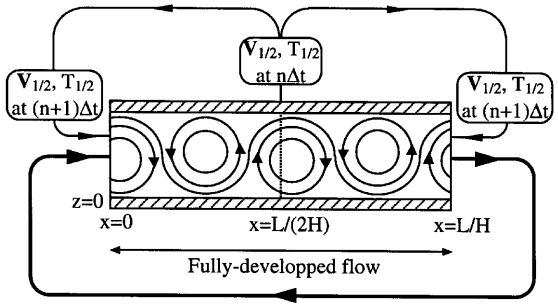

Figure 4. Second computational configuration—simulation of periodic boundary conditions

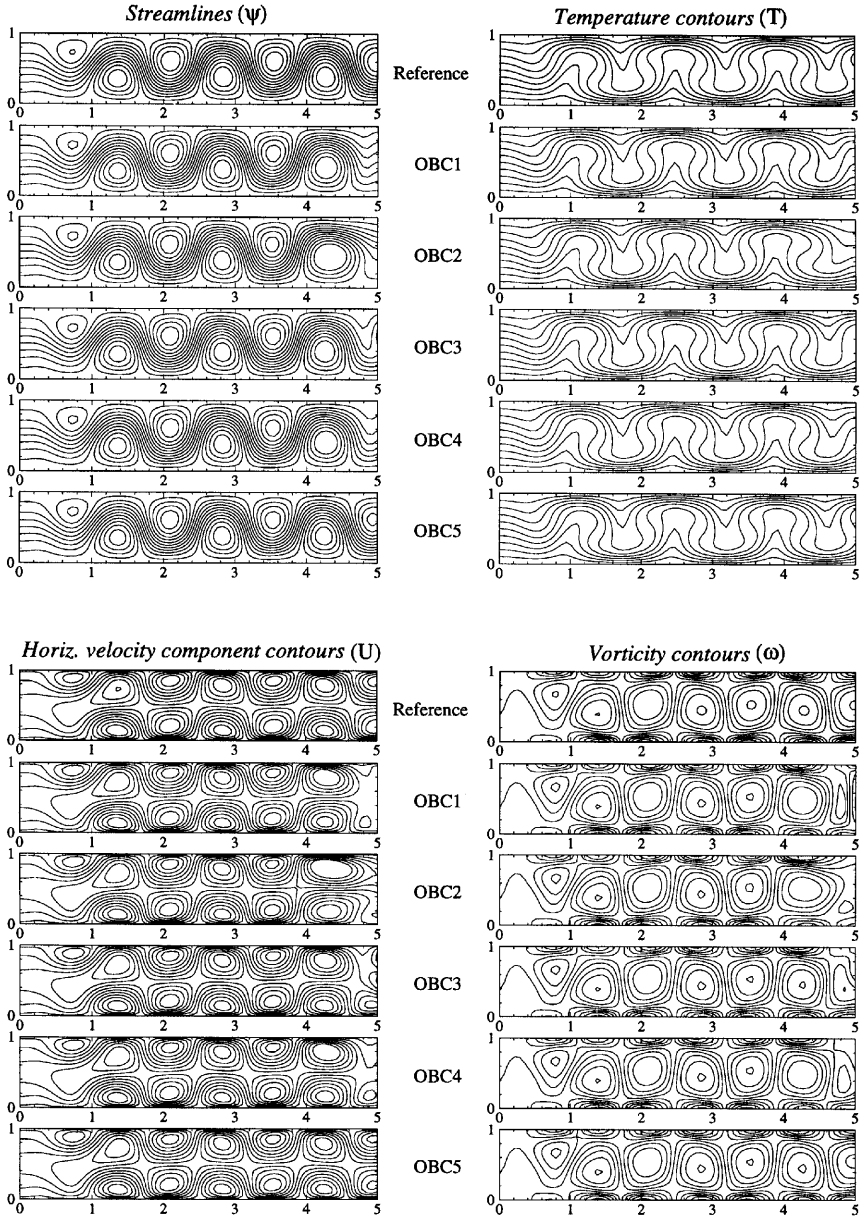

Figure 5. Field plots for different OBC treatments at time t^* ($Ra = 10{,}000$, $Re = 10$ and $Pr = \frac{2}{3}$)

the convective roll which goes out from the numerical domain goes into it on the opposite side. The top and bottom boundary conditions as well as the initial conditions are the same as those of the first configuration (see Table I). Note that because of the special way of proceeding, the number of transversal rolls in the computational domain is necessarily a multiple of four. Therefore the transversal roll wavelength λ is imposed by the aspect ratio L/H. In Evans and Paolucci's benchmark

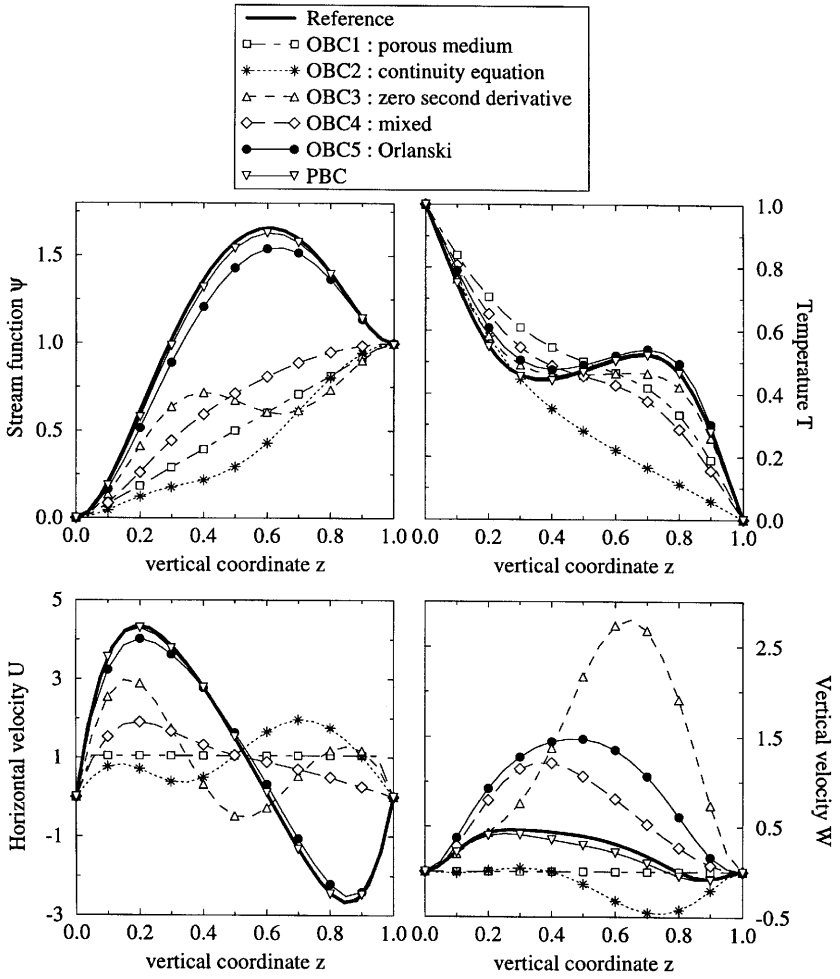

Figure 6. Field profiles at outlet boundary at time t^* for different OBCs and PBCs

case,[17] characterized by $Ra = 10{,}000$, $Re = 10$ and $Pr = \frac{2}{3}$, it was shown that $\lambda \approx 1{\cdot}44$. Thus for the simulation with PBCs a channel with $L/H = 2{\cdot}88$ has been chosen so that four transversal rolls with the right wavelength appear in the duct; in this case the steps in space are $(\Delta x, \Delta z) = (0{\cdot}0725, 0{\cdot}05)$.

RESULTS AND DISCUSSION

The results obtained with the five OBCs are compared with a reference solution for each set of Rayleigh, Reynolds and Prandtl numbers. These solutions are called 'Reference' in all the figures and tables. They are computed over domains twice as long as those used to test the OBCs and only their first half is taken into account. Indeed, the perturbation due to the OBC at the outlet of the channel is supposed to be negligible on this first half. For the Reference the grid is finer and the OBC used is OBC5.

In the first step all the tests are carried out for the case proposed by Evans and Paolucci. The Reference is computed on a domain of aspect ratio 10 with $(\Delta x, \Delta z) = (0{\cdot}05, 0{\cdot}0385)$. Figure 5 permits us to compare the streamlines, isotherms, iso-values of horizontal velocity component and

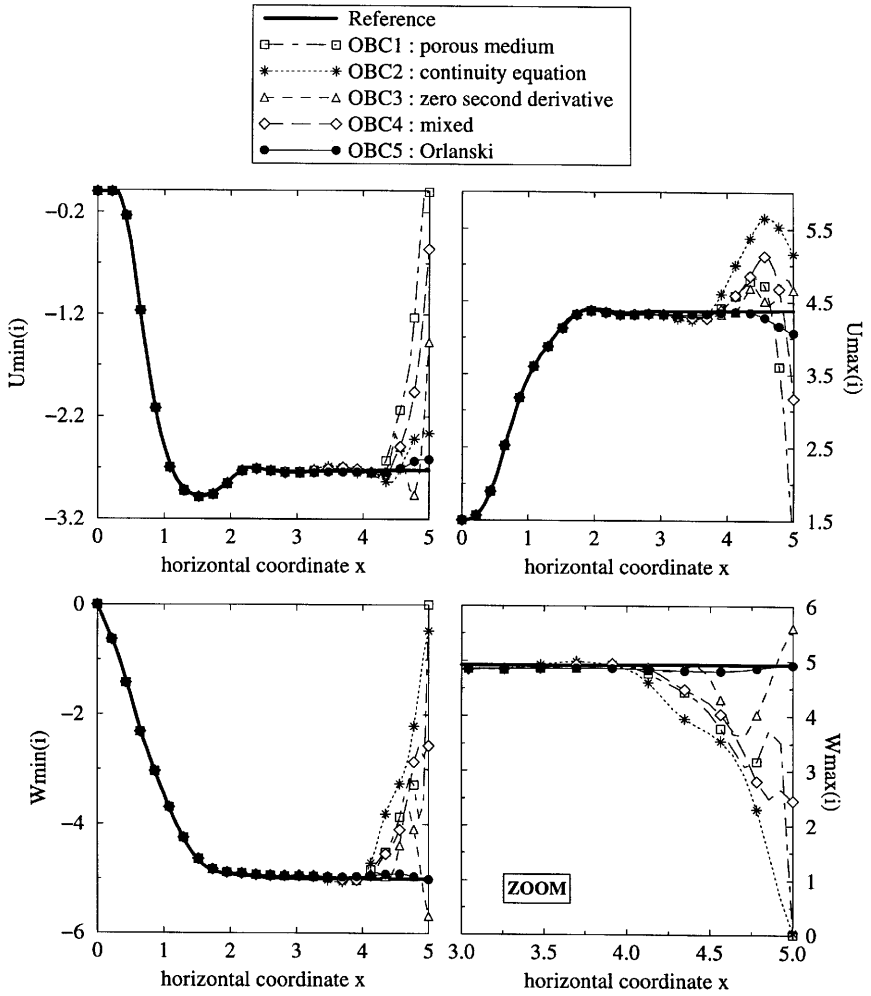

Figure 7. Envelopes of U and W extrema along axis of channel; visualization of perturbed zone for the different tested OBCs ($Ra = 10000$, $Re = 10$ and $Pr = \frac{2}{3}$)

iso-vorticity contours obtained with the different OBCs and with the Reference. Each solution is recorded at the same time t^*, defined as the time when the temperature reaches a local minimum at the fixed position $(x, z) = (L - \frac{5}{4}\lambda, H/2)$, where λ is the roll wavelength ($\lambda = 1{\cdot}44$). From the OBC point of view this is the most unfavourable time, since this is the moment when a thermoconvective roll sits astride the outlet boundary: nearly half of this boundary is submitted to an entrance flow. This is also the most interesting time to evaluate the behaviour of the OBCs faced with return flows. Figure 5 shows that the solution is very perturbed by OBC1, OBC2, OBC3 and OBC4, whereas OBC5 seems to allow a good undisturbed evacuation of the transversal rolls.

To focus on the perturbation at the outlet boundary, Figure 6 presents the ψ, T, U and W vertical profiles at $x = L/H$ for each OBC and for the PBCs compared with the Reference (where ψ is the streamfunction). The recording time is t^* as before. The profiles which are furthest from the reference solution are obtained with OBC2; the behaviours of OBC1, OBC3 and OBC4 are not very good either. On the other hand, OBC5 behaves almost like the Reference (except for W). OBC5 is also the

Table II. Comparison of flow parameters obtained with different OBCs and with Reference values for $Ra = 10{,}000$, $Re = 10$ and $Pr = \frac{2}{3}$. The percentages give the discrepancy with respect to the Reference

	λ	τ	$\langle\overline{Nu}\rangle$	Umin	Umax	Wmin	Wmax
Evans and Paolucci[17]	1·4465	1·3319		−2·6495	4·3958	−5·0587	5·0319
Reference	1·439	1·298	2·643	−2·720	4·380	−5·002	4·929
OBC1	1·413	1·298	2·578	0	1·05	0	0
				(100%)	(76%)	(100%)	(100%)
OBC2	1·419	1·296	2·537	−2·348	5·653	−0·469	0·045
				(14%)	(29%)	(91%)	(99%)
OBC3	1·419	1·298	2·638	−1·474	4·828	−3·741	3·641
				(46%)	(10%)	(25%)	(26%)
OBC4	1·406	1·298	2·582	−0·558	3·174	−2·559	2·456
				(80%)	(28%)	(49%)	(50%)
OBC5	1·425	1·296	2·649	−2·616	4·072	−4·909	4·814
				(4%)	(7%)	(2%)	(2%)
PBC	1·440	1·310	2·662	−2·741	4·358	−4·951	4·859
				(0·8%)	(0·5%)	(1%)	(1·4%)

only boundary condition, with OBC3 to a lesser degree, which allows a clear return flow, i.e. a negative horizontal velocity component. The good agreement between the PBCs and the Reference can be noted too. Generally speaking, all the results obtained with PBCs describe very well the behaviour of the transversal rolls.

The minimum and maximum values of U and W in the course of time in each vertical section (i) of the duct are presented in Figure 7. More precisely, this figure shows $U\min(i)$, $U\max(i)$, $W\min(i)$ and $W\max(i)$ as a function of x, where

$$U\min(i) = \min_{t=0,Nt}\left(\min_{k=0,Nz} U(i,k)\right), \qquad U\max(i) = \max_{t=0,Nt}\left(\max_{k=0,Nz} U(i,k)\right),$$

$$W\min(i) = \min_{t=0,Nt}\left(\min_{k=0,Nz+1} W(i,k)\right), \qquad W\max(i) = \max_{t=0,Nt}\left(\max_{k=0,Nz+1} W(i,k)\right),$$

i and k are the horizontal and the vertical space index respectively, Nt is the total number of time iterations and Nz is the total number of meshes in the z-direction. In this way the envelopes that are obtained illustrate clearly the magnitude of the perturbation and the length of the perturbed zone for each OBC. The amplitude of the perturbation varies significantly from one OBC to another; for instance, compared with the Reference, the amplitude of the perturbation is less than 7% for OBC5 and reaches 100% for OBC1 and OBC2. The length of the perturbed zone is more difficult to determine precisely, because the perturbations propagate upstream oscillating slightly. Nevertheless, for the present flow the length of the perturbed zone varies approximately between H for OBC5 and $1{\cdot}5H$ for OBC2.

Figure 7 is also a good means to evaluate the length of the entrance zone. It is approximately $2H$ long. Thus for $x \geqslant 2$ the convective flow of transversal rolls can be considered as being established. Table II presents several physical parameters computed in this zone and characterizing the thermoconvective flow. These parameters are the wavelength λ and time period τ of the transversal rolls and the space and time average Nusselt number $\langle\overline{Nu}\rangle$ on the bottom and top plates of the channel:

$$\langle\overline{Nu}\rangle = \frac{1}{Nt\Delta t}\int_0^{Nt\Delta t} \overline{Nu}(t)\mathrm{d}t,$$

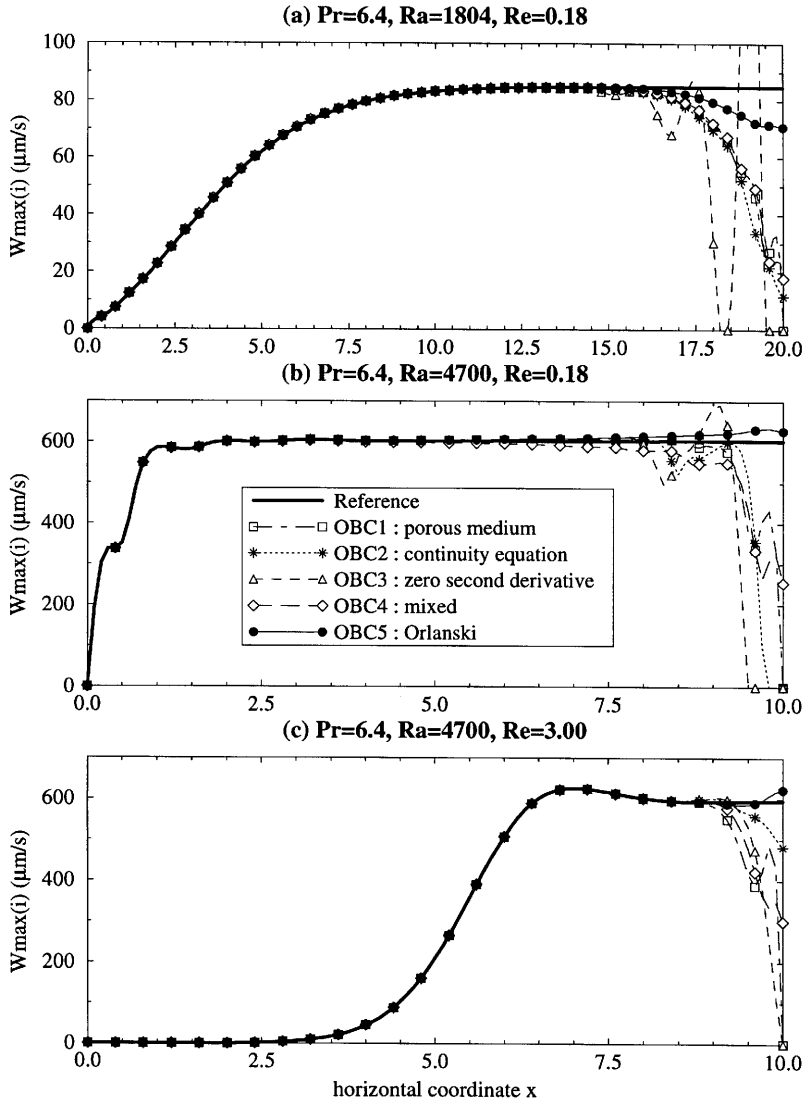

Figure 8. OBC effect upon envelope of vertical velocity component as a function of Rayleigh and Reynolds numbers

where

$$\overline{Nu}(t) = \frac{1}{L/H - 2} \int_2^{L/H} \frac{1}{2} \left[\left(\frac{\partial T}{\partial z} \right)_{z=0^+} (x, t) + \left(\frac{\partial T}{\partial z} \right)_{z=1^-} (x, t) \right] \mathrm{d}x.$$

The values of $U\min(i)$, $U\max(i)$, $W\min(i)$ and $W\max(i)$ the furthest from the Reference, for $x = 2$ to L/H, are also given; these values are respectively denoted Umin, Umax, Wmin and Wmax and the discrepancies with respect to the Reference are given as a percentage below each value. All these results (except $\langle \overline{Nu} \rangle$) obtained for the five OBCs and the PBCs are compared with the benchmark of Evans and Paolucci.[17]

From Table II it appears that the internal structure of the flow is not modified by the choice of the OBCs. Indeed, taking into account the margin of error on the measurements ($\pm 0{\cdot}1$ on λ and $\pm 0{\cdot}001$ on τ), the wavelength and time period of the transversal rolls do not vary as a function of the OBCs; the fluctuations of the Nusselt number are negligible too. On the other hand, the variations in the velocity can be locally very important; the discrepancies of Umin, Umax, Wmin and Wmax with respect to the Reference are small only with OBC5 and with the PBCs.

The influence of the OBCs as a function of Ra and Re is studied for flows corresponding to the experiments of Ouazzani *et al.*,[10] i.e. for water flows ($Pr = 6{\cdot}4$) at an average temperature of 23°C ($\nu = 0{\cdot}93 \times 10^{-6}$ m^2 s^{-1}) in a duct of height $H = 4{\cdot}15$ mm. In this aim, Figure 8 gives $W\max(i)$ as a function of x for three combinations of Ra and Re; $W\max(i)$ is plotted dimensionally. $Ra = 1804$ is close to the critical Rayleigh number Ra^* characterizing the onset of thermoconvection in the Poiseuille–Bénard flow. Note that the appearance of fully established thermoconvective rolls is rejected far from the inlet ($x \approx 7$) when $Re = 3$ for $Ra = 4700$ (see Figure 8(c)). When the Rayleigh number is smaller (e.g. $Ra = 1804$) and $Re = 3$, the thermoconvective rolls cannot appear in the channel at $Pr = 6{\cdot}4$.[10]

Whatever the combination of Ra and Re, the smallest amplitude of perturbation is always obtained with OBC5. The behaviour of the flow with OBC1, OBC2 and OBC4 is approximately the same (especially at $Ra = 1804$, Figure 8(a)). The behaviour of OBC3 is different: the perturbation oscillates at the smallest Reynolds number $Re = 0{\cdot}18$ (Figures 8(a) and 8(b)), particularly when $Ra = 1804$. As it has already been shown in the case of the flow of Evans and Paolucci, the length of the perturbed zone varies very little from one OBC to another. On the other hand, it varies with Ra and Re: it is around $5H$ in Figure 8(a) for $Ra = 1804$ and $Re = 0{\cdot}18$, around $3H$ in Figure 8(b) for $Ra = 4700$ and $Re = 0{\cdot}18$ (a bit more for OBC4) and around H in Figure 8(b) for $Ra = 4700$ and $Re = 3$.

The fact that the length of the perturbed zone increases when Ra diminishes is in good agreement with the linear theory. The latter predicts,[4] in the case of free convection (i.e. with rigid boundaries at the outlet), that the length necessary to obtain fully developed thermoconvective rolls varies as $[(Ra - Ra^*)/Ra^*]^{-1/2}$: therefore near the boundaries the length in question tends to infinity when Ra tends to Ra^* (with $Ra > Ra^*$). The length of the perturbed zone also increases when Re diminishes, because the perturbations caused by the OBCs can go upstream all the more easily as the forced convection is weak.

CONCLUSIONS

In the first part of this paper the implementation details of the algorithm based on the augmented Lagrangian method are given; the implementation of the different open boundary conditions (OBCs) and of the periodic boundary conditions (PBCs) is also described.

The second part is dedicated to the analysis of the response of the Poiseuille–Bénard channel flow (PBCF) solved with the five different OBCs. In particular, comparison criteria are introduced to finely evaluate the amplitude of the perturbation and the length of the perturbed zone at the outlet boundary of the computational domain. The results show the very good behaviour of the flow when Orlanski-type boundary conditions (OBC5) are used at the outlet; they also show that the flow is comparatively very perturbed with the other four OBCs. On the other hand, the PBCs give excellent results; they also allow us to reduce the length of the computational domain (and subsequently to save on storage and computing time), since it is possible to work with only two space periods of the thermoconvective flow.

It is shown that the improvement obtained with OBC5 is due to the important reduction of the amplitude of the perturbation without any significant reduction of the length of the perturbed zone. The latter remains approximately constant whatever the OBC used. It is also shown that the length of

the perturbed zone can vary from H to $5H$ with Ra and Re; the length increases when Ra and Re diminish.

ACKNOWLEDGEMENTS

The numerical simulations for the present work were performed on the IBM-SP2 computer of the CNUSC (South University National Centre of Computation). The authors would like to thank the staff of the CNUSC for their technical support and training.

REFERENCES

1. Y. Mori and Y. Uchida, 'Forced convective heat transfer between horizontal flat plates', *Int. J. Heat Mass Transfer*, **9**, 803–817 (1966).
2. K. S. Gage and W. H. Reid, 'The stability of thermally stratified plane Poiseuille flow', *J. Fluid Mech.*, **33**, 21–32 (1968).
3. K. C. Cheng and R. S. Wu, 'Axial heat conduction effects on thermal instability of horizontal plane Poiseuille flows heated from below', *J. Heat Transfer*, **98**, 564–569 (1976).
4. J. K. Platten and J. C. Legros, *Convection in Liquids*, Springer, Berlin, 1984.
5. H. W. Müller, M. Lücke and M. Kamps, 'Convective patterns in horizontal flow', *Europhys. Lett.*, **10**, 451–456 (1989).
6. H. R. Brand, R. J. Deissler and G. Ahlers, 'Simple model for the Bénard instability with horizontal flow near threshold', *Phys. Rev. A*, **43**, 4262–4268 (1991).
7. H. W. Müller, M. Tveitereid and S. Trainoff, 'Rayleigh–Bénard problem with imposed weak through-flow: two coupled Ginzburg–Landau equations', *Phys. Rev. E*, **48**, 263–272 (1993).
8. J. M. Luijkx, J. K. Platten and J. C. Legros, 'On the existence of thermoconvective rolls, transverse to a superimposed mean Poiseuille flow', *Int. J. Heat Mass Transfer*, **24**, 803–817 (1981).
9. M. T. Ouazzani, J. P. Caltagirone, G. Meyer and A. Mojtabi, 'Etude numérique et expérimentale de la convection mixte entre deux plans horizontaux à températures différentes', *Int. J. Heat Mass Transfer*, **32**, 261–269 (1989).
10. M. T. Ouazzani, J. K. Platten and A. Mojtabi, 'Etude expérimentale de la convection mixte entre deux plans horizontaux à températures différentes—2', *Int. J. Heat Mass Transfer*, **33**, 1417–1427 (1990).
11. M. T. Ouazzani, J. K. Platten and A. Mojtabi, 'Intermittent patterns in mixed convection', *Appl. Sci. Res.*, **51**, 677–685 (1993).
12. E. Schröder and K. Bühler, 'Three-dimensional convection in rectangular domains with horizontal throughflow', *Int. J. Heat Mass Transfer*, **38**, 1249–1259 (1995).
13. S. S. Chen and A. S. Lavine, 'Laminar, buoyancy induced flow structures in a bottom heated, aspect ratio 2 duct with throughflow', *Int. J. Heat Mass Transfer*, **39**, 1–11 (1996).
14. H. K. Moffat and K. F. Jensen, 'Complex flow phenomena in MOCVD reactors—1. Horizontal reactors', *J. Cryst. Growth*, **77**, 108–119 (1986).
15. G. Evans and R. Greif, 'Unsteady three-dimensional mixed convection in a heated horizontal channel with applications to chemical vapour deposition', *Int. J. Heat Mass Transfer*, **34**, 2039–2051 (1991).
16. G. Evans and R. Greif, 'Thermally unstable convection with applications to chemical vapour deposition channel reactors', *Int. J. Heat Mass Transfer*, **36**, 2769–2781 (1993).
17. G. Evans and S. Paolucci, 'The thermoconvective instability of a plane Poiseuille flow heated from below: a proposed benchmark solution for open boundary flows', *Int. j. numer. methods fluids*, **11**, 1001–1013 (1990).
18. R. L. Sani and P. M. Gresho, 'Résumé and remarks on the open boundary condition minisymposium', *Int. j. numer. methods fluids*, **18**, 983–1008 (1994).
19. A. Bottaro, 'Note on open boundary conditions for elliptic flows', *Numer. Heat Transfer B*, **18**, 243–256 (1990).
20. M. H. Kobayashi, J. C. F. Pereira and J. M. M. Sousa, 'Comparison of several open boundary numerical treatments for laminar recirculating flows', *Int. j. numer. methods fluids*, **16**, 403–419 (1993).
21. H. Uzawa, 'Iterative methods for concave programming', in K. J. Arrow, L. Hurwicz and H. Uzawa (eds), *Studies in Linear and Nonlinear Programming*, Stanford University Press, Stanford, CA, 1958, pp. 154–165.
22. R. Temam, *Navier–Stokes equations—Theory and Numerical Analysis*, North-Holland/Elsevier, Amsterdam, 1977.
23. M. Fortin and R. Glowinski, *Méthodes de Lagrangien Augmenté*, Dunod, Paris, 1982.
24. R. Glowinski, *Numerical Methods for Nonlinear Variational Problems*, Springer, New York, 1984.
25. K. Khadra, 'Méthode adaptative de raffinement local multigrille—application aux équations de Navier–Stokes et de l'énergie', *Ph.D. Thesis*, University of Bordeaux I, 1994.
26. P. Traore, 'Contribution numérique à l'étude des transferts couplés de quantité de mouvement, de chaleur et de masse dans un jet semi-confiné', *Ph.D. Thesis*, University of Toulouse III, 1996.
27. H. A. Van Der Vorst, 'Bi-CGSTAB: a fast and smoothly converging variant of Bi-CG for the solution of nonsymmetric linear systems', *SIAM J. Sci. Stat. Comput.*, **13**, 631–644 (1992).

28. I. Gustafsson, 'On first and second order symmetric factorization methods for the solution of elliptic difference equations', Chalmers University of Technology, 1978.
29. S. V. Patankar, *Numerical Heat Transfer and Fluid Flow*, Stockholm, Washington, DC, 1980.
30. I. Orlanski, 'A simple boundary condition for unbounded hyperbolic flows', *J. Comput. Phys.*, **21**, 251–269 (1976).

